Fundamental and Magnetic Force Analysis of an External Rotor Switched Reluctance Motor

H. Torkaman, N. Arbab, H. Karim, and E. Afjei

Department of Electrical and Computer Engineering, Shahid Beheshti University, G.C. Tehran, Iran
Emails: H_Torkaman@sbu.ac.ir, Arbab.nasim@gmail.com, H-Karim@ieee.org, E_Afjei@sbu.ac.ir

Abstract ─ This paper presents a novel three-phase 6/8 external rotor switched reluctance motor. Such a construction not only leads to reduce the total weight and volume, but also increases the total efficiency in a small size motor. Three dimensional finite element method is applied to evaluate the main characteristics of the proposed motor such as magnetic flux density, flux linkage, self-inductance, mutual inductance, and output torque. Moreover, this paper investigates the radial force components of the motor. This assessment is carried out under different forced current levels with the respect to critical rotor positions. From the motor analysis results, it is considered that the proposed motor has great advantages over the conventional type in its magnetic profiles.

Index Terms ─ External rotor configuration, radial force, switched reluctance motor, three dimensional finite element method.

I. INTRODUCTION

The salient features of a switched reluctance motor (SRM) such as the lack of a coil or a permanent magnet on the rotor, a simple structure and high reliability, makes it a suitable candidate for operation in harsh or sensitive applications [1, 2]. However, due to the operation in the magnetic saturation region, the high performance torque control of this type of motor is a critical issue for smooth running. A comprehensive magneto static modeling and analysis in different conditions can improve the operating performance for the entire motor control system [3-6].

In general, there are four distinct types of SRMs: namely, regular doubly salient cylindrical [7], disc-type [8], multi-layer, and linear motors [9]. This classification stems from the general shape of the motor. The regular cylindrical type of SR motor has salient poles on both stator and rotor, and the windings are wrapped around the stator poles. Direct current motors with disc rotors are widely used and have been proposed for SR motors as well. The need for disc type arises in applications where the spacing is of the primary concern. The multilayer SR motor consists of three magnetically independent layers or phases. Each layer comprises of a stationary part and a rotating piece known as stator and rotor, respectively.

Regarding the conventional design, the air gap radius is limited by the space needed for the coils inside the stator furthermore by the cooling inside the housing surrounding the laminations. The external rotor design has the benefit that coils and cooling can be placed near the shaft, increasing the possible air gap radius [10]. As a result, the external rotor switched reluctance motors (ERSRM) own the comparative advantage of having higher output torque at low speed and also elevated motor efficiency. Additionally, ERSRMs are suitable in-wheel motors for electric vehicles (EVs) because they provide great flexibility in motion control [11].

Basis of ERSRMs is on tendency of the polarized rotor pole in achieving full alignment position with the excited stator pole which provokes a whirling mode of the motor [8, 12]. Tangential and radial forces are two components of this magnetism force. The tangential force transforms into the rotational torque. Generally, in balanced motor operation, the total of radial force is zero at ideal mode. However, faulty operation caused by structural or environmental motivations gives rise to unbalance radial forces which are undesired and they result in motor vibrations. For instance, unbalanced external load or off-centered rotor leads to form asymmetrical air gap and then acoustic noise of the motor, due to produced radial force [13].

Submitted On: February 16, 2011
Accepted On: October 20, 2011

Authors in the previous works have proposed several SRM structures such as; a new multilayer SRM [14], a novel field assisted SRM/G [15], and also in [16] a novel switched reluctance generator (SRG) is compared with a BLDC. Furthermore, the magnetic characteristics of the various SRMs are evaluated in [17-23] under normal and faulty conditions. Therefore, in this paper, the magnetic profiles of the new SRM with external rotor are obtained and analyzed. In this regard, due to nonlinear and complex magnetic treatments of SRMs, three dimensional finite element method (3D-FEM) is utilized for precise analysis and evaluation of the magnetic characteristics.

II. THE ERSRM STRUCTURE

As stated before, the purpose of this paper is to evaluate a small size switched reluctance motor with an external rotor. A proper design method for the SRM is imperative to overcome its disadvantages. The suitable method will definitely improve the potentials of SRM in various adjustable speed drive applications. Like other motors, the SRM has specific characteristics that make it appropriate for certain applications and inappropriate for others. The degree of appropriateness of a SRM for any application depends on the objectives and application's requirements.

The analytical design equation and some specific ratios for this study, are adapted from [24] and the IEC71 standard. These design equations are used to evaluate different SRM traits considering magnetic saturation. The approximations and some simplifications are adopted during the development of analytical design equations are vindicated with FEM analysis. It is worth to be pointed out that the maximum torque density, minimum flux leakage, and efficiency are among the various design objectives in this study.

In this motor, the stator and rotor cores are made by non-oriented steel lamination to reduce the eddy current effects and skin effects as well as hysteresis losses. The laminations of the stator and rotor and their dimensions are shown in Fig. 1 and Table I, respectively.

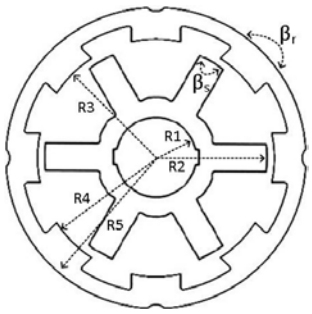

Fig. 1. The lamination and dimensions of proposed ERSRM.

Table 1. The dimensions of proposed ERSRM

Parameters	value
Number of phases	3
R1	8 mm
R2	22.2 mm
R3	22.5 mm
R4	25.5 mm
R5	28.5 mm
βs	14.5˚
βr	24˚
Minimum air gap	0.3 mm

ERSRM consists of eight salient poles in rotor with no windings, while the stator has six salient poles which include windings wrapped around them. In this type of SRM, rotor is placed outside instead of the stator; both stator and rotor have salient poles such as conventional SRMs. Based on this structure, the motor named 6/8 ERSRM.

III. FEM MODELING AND RESULTS

To evaluate the motor design and performance properly, a reliable model is required. The FEM can be conveniently used to obtain the magnetic vector potential values throughout the motor in the presence of complex magnetic circuit geometry and nonlinear properties of the magnetic materials. These vector potential values can be processed to obtain the field distribution, torque, and flux leakage. In this paper, the field analysis was performed using a Magnet CAD package [25]. This package is based on the variation energy minimization technique to solve for the magnetic vector potential. The technique utilized by the MagNet package is based on the variational energy minimization technique to solve for the electric vector potential. In this method, the electric vector potential is known as $T-\Omega$ formulation.

Magnetic flux density is derived for different rotor position through a variety of forced currents.

The amplitude of magnetic flux density for 2A forced current is shown in Fig. 2 at different critical positions (unaligned, half aligned, and fully aligned positions).

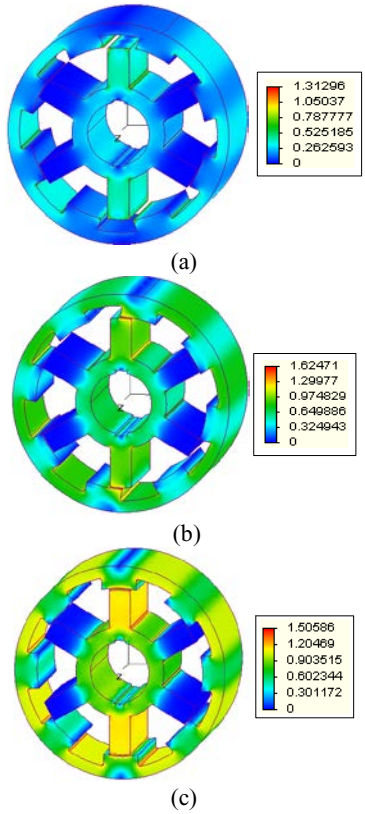

Fig. 2. Flux density distribution at: a) unaligned, b) half aligned, and c) fully aligned positions.

As seen from Fig. 2, when rotor moves from an unaligned position to a half aligned position, the maximum flux densities in stator/rotor poles are increased from 0.65 to 1.62 Tesla; it means the flux density in a half aligned position is 2.5 times higher than an unaligned position. It shows the power of the generation axial force between stator and rotor poles. This fact helps us to produce high torque value and improved motor speed.

In an SRM, inductance is a function of rotor position and stator current. At an aligned position or at higher current levels, the ferromagnetic material in the stator and rotor poles begins to saturate. As a result of the secondary effects such as saturation, fringing, and leakage, nonlinearities are introduced in the connection between inductance, rotor position, and current. At an unaligned position, phase inductance has a minimum value due to high reluctance offered by large air gap. Magnetic saturation is unlikely to occur at an unaligned position, and thus, the flux linkage shows a linear behavior until the start of overlap. Where rotor poles completely overlap with stator poles, at a fully aligned position, magnetic field density tends to saturate at high current levels. It makes flux linkage a nonlinear function of position and stator current. This behaviour is shown in Fig. 3.

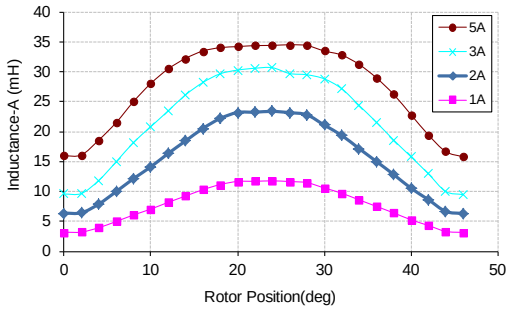

Fig. 3. Self-inductance of phase A vs. rotor position under various forced currents.

As shown in Fig. 3, with increasing forced current from 1 to 5 Amperes, the self-inductance in phase A goes up from 12 to 35mH (in maximum value). Furthermore, it illustrates the shape of inductance in the low currents is linear but in high current is nonlinear because of saturation phenomena. As seen from Fig. 3, by exciting at the position where the slope of inductance always increases, the ERSRM always produces high positive torque and can rotate continuously with minimum ripple.

Suppose two coils are placed near each other, the same as coils in the proposed motor. Since the two coils are close to each other, some of the magnetic field lines through the former coil will also pass through the other coil. As a result, there will be an induced electro motive force associated with the changing magnetic flux in the second coil. The fact that a change in the current of a coil affects the voltage and current in another coil is defined as mutual inductance. In a proposed motor, when phase A is excited and two other phases are off, mutual inductance appears in two other inactive phases (B,C) as shown in Figs. 4 and 5.

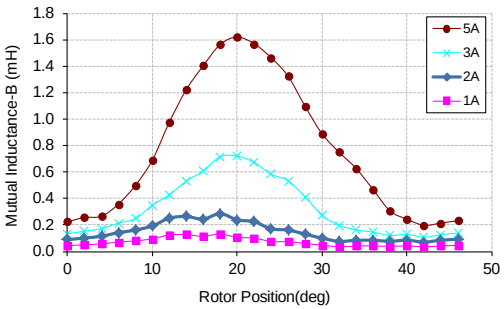

Fig. 4. Mutual inductance of phase B vs. rotor position under various forced currents.

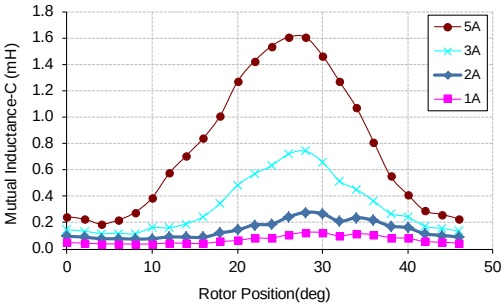

Fig. 5. Mutual inductance of phase C vs. rotor position under various forced currents.

As it is depicted from Figs. 4 and 5, the mutual inductances in coils B1, B2, C1, and C2 have very low amplitude, as the maximum mutual inductance is 1.6mH in 5A forced current. In addition, the mutual inductances in inactive phases are decreased when the current has descended. It is mentionable that this feature is very promising in this type of machine than conventional SRM to decrease the losses and improve the efficiency.

On the other side, the ratio of mutual inductance in inactive phases respect to self-inductance in active phase (A) is considerable in this machine. Figures 3 and 5 demonstrate with an increase in forced current, the produced mutual inductance in the phase B respect to self-inductance in phase A (in maximum value of $(L_{B1}/L_{A1})\times 100\%)$ increases from 0.7% to a maximum of 4.5% (for $i=0.1A$ to $i=5A$). Similarly, this manner is repeated in the phase C respect to phase A. This means the induced flux to inactive phases in idle mode have very low amplitude which it has originated from structure and dimension of the designed ERSRM. In motor designs, the inductance ratio (mutual inductance/ self-inductance) should be minimized, so the proposed ERSRM is usually guaranteed for a well-designed motor.

In a SRM, inductance and reluctance are functions of a phase current, which causes the establishment of flux and rotational motion. At an aligned position and higher current levels, magnetic iron begins to saturate. Due to saturation, fringing, and leakage, nonlinearities are introduced. At an unaligned position, phase inductance has minimum value as a result of high reluctance presented by large air gap. Since the stator and rotor poles overlap, pole corners display local saturation due to concentration of flux into the relatively small area of the pole corners and hence flux linkage curve begin to be nonlinear. When rotor poles completely overlap with stator poles, at fully aligned position, stator/rotor poles and stator yoke saturate at high current levels making flux linkage a nonlinear function of position and current.

Saturation effects tend to lower the aligned inductance, which in effect, decreases the rate of change of inductance. As torque is proportional to slope of inductance, saturation lowers the torque produced at given current on one hand; while on other hands it improves the ratio of mechanical energy to the energy supplied by a controller. For the numerical calculation of torque, this paper uses the flux profiles obtained from 3D-FEM simulations and measurements.

Based on the fundamentals of torque concept, Fig. 6 shows the static torque profiles for the ERSRM from 1 to 5 A.

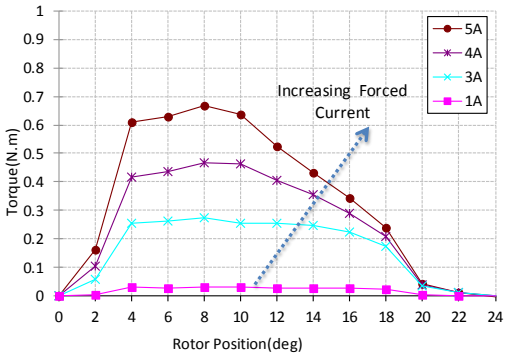

Fig. 6. Static torque vs. rotor position under various forced currents.

As expected from torque equations, rising current must result in a linear increase in torque, but as it is shown in Fig. 6, it does not. Because, the stator/pole cores are imported in the

nonlinearly region in high amplitude of current and motor is operating in the saturation zone.

It is shown, the torque per ampere ration in this motor is good for this volume. It is worthy to mention that the increment of torque per ampere ratio reduces the volt-ampere which is required for the motor control converter.

As seen from Fig. 6, higher torque curve has been obtained for the 5A current. This means, with increasing the forced current the torque will be increased, also its ripple will be greater than before. In solving this issue, the controller unit as well as switching angle must be modified. Also, considering the maximum torque per ampere for control strategy leads to smooth torque control of an ERSRM.

IV. Magnetic Force Characteristic Analysis

The predicted radial and tangential force characteristics of the ERSRM are presented by this part. First of all, some descriptions of these forces calculation should be pointed out. The calculations of the radial forces are based on Maxwell stress tensor. The radial and tangential forces based on Maxwell stress tensor are given by (1), and (2), respectively.

$$f_n = \frac{1}{2\mu_0}(B_n^2 - B_t^2), \quad (1)$$

$$f_t = \frac{1}{2\mu_0} B_n B_t, \quad (2)$$

where f_n, f_t are the produced radial and tangential forces, respectively. The B_n, B_t and μ_0 are the normal component, the tangential component of the flux densities, and the absolute permeability, respectively.

It can be concluded that the B_n and B_t should be equal in healthy motor and ideal condition, which results in zero value for their differences as well as radial force. This ideal condition does not appear in all machines, because of their asymmetric structure, assembly errors, and load fluctuations. Therefore, it is noticeable that the maintaining of radial force in minimum value is essential to avoid producing noise and vibration.

According to equation (2), it can be predicted that the maximum radial force occurs at the fully aligned position since the radial field component reaches its maximum value while the tangential field component is on its minimum value. In order to achieve the accurate results from this method, a circle contour was chosen in the middle of the air gap. It is worth noting that the resulted force is independent of the integration path. Maxwell's equations indicate that studying the components of the flux density is crucial in order to understand the force generation process.

For the first step of this analysis, the variations of radial field component versus contour position under different forced currents are calculated for ERSRM. These profiles are shown in Fig. 7, for unaligned, half aligned, and fully aligned rotor positions.

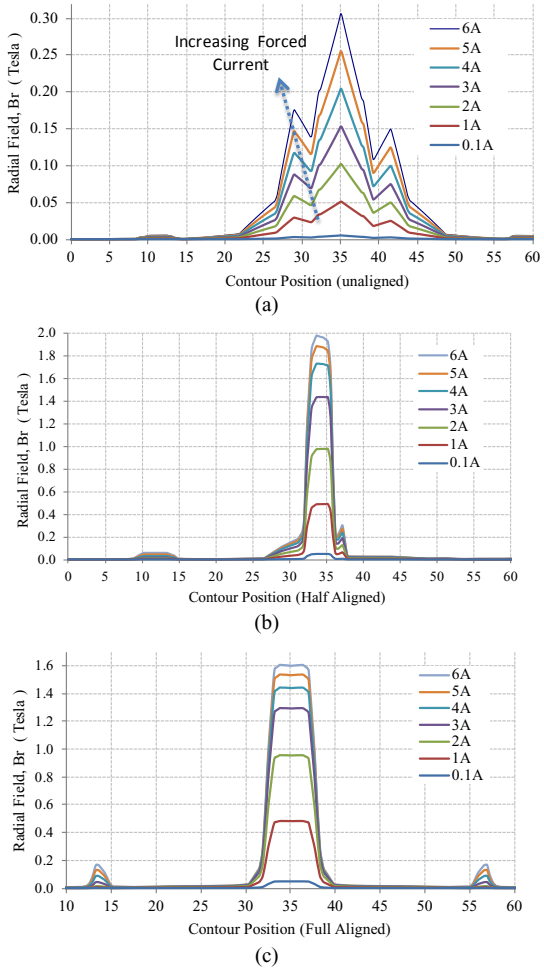

Fig. 7. Radial field component vs. contour position under different forced currents: a) unaligned, b) half, and c) fully aligned positions.

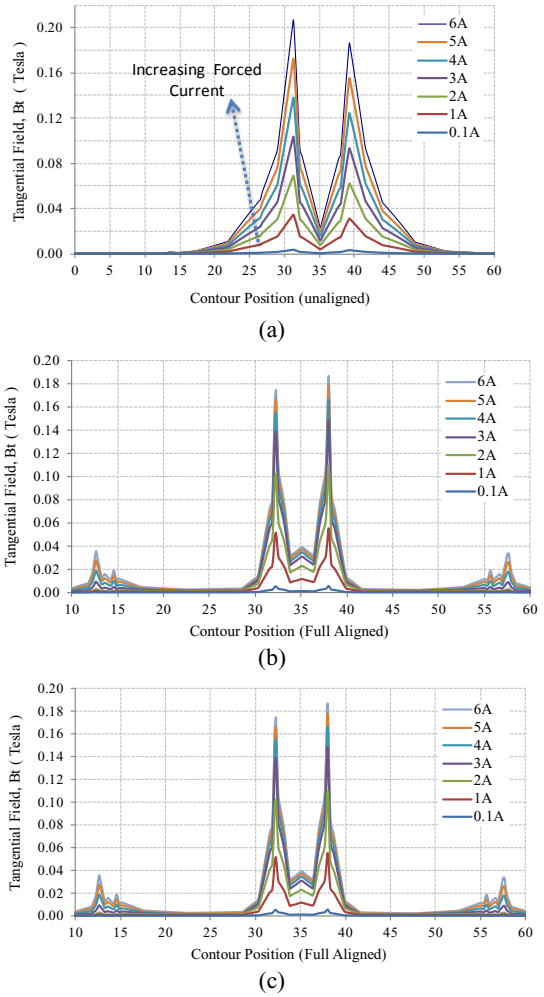

Fig. 8. Tangential field component vs. contour position under different forced currents: a) unaligned, b) half, and c) fully aligned positions.

The variations of tangential field component versus contour position under different forced currents are calculated for ERSRM. These profiles are shown in Fig. 8, for unaligned, half aligned, and fully aligned rotor positions.

As the results of Fig. 8 demonstrate, the maximum of B_t occurs at respective corner tips of stator and rotor. Notably, effects of local saturation at these rotor and stator tips result in two local maxima in B_t. It is important to note that a largely normal force exists at this rotor position that is substantially stronger than a tangential component. As shown in Fig. 7, the amplitude of the radial field component increases nonlinearly. In fact, as the forced current enhances, the amplitude of B_t and B_n are increased more slowly due to the saturation effect. Radial field components (B_n) in an unaligned position rises with current, but the amplitude is very low namely 0.301 Tesla and is on its maximum value when the forced current is fixed at 6A.

As the rotor leaves the unaligned position toward the half aligned position, the overlap between rotor and stator poles begins. Hence, effects of local saturation are visible in the first and second peak of Fig. 8. As it is shown, the first peak decreases with the ratio of 0.76, and the second peak increases with the ratio of 1.6. As rotor leaves the half aligned position toward the fully aligned position, the maximum value of radial field component remains almost constant (in higher currents the amplitude decreases with the 0.8 ratio). Although the maximum value of radial field stays almost constant or decreases in higher currents, the width of the region within which the radial component exists increases. It means that the average radial force has its own maximum value at fully aligned position as it was expected.

Figure 9 shows the variations of total produced radial forces under 1, 4, 5, and 6 Amperes forced currents in ERSRM.

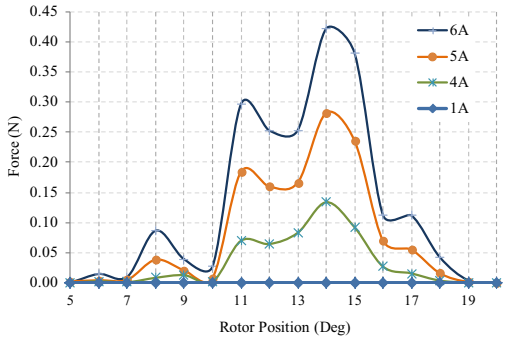

Fig. 9. Radial force vs. rotor position under different forced currents.

According to Fig. 9, it is realized that, the amplitude of the radial force is almost zero in the low level of forced current. Besides, when the level of the forced current is increased from 4 to 5 and 6A the maximum radial force has 2 and 3 times higher value than 4A current.

As it was mentioned in previous sections, the radial force produced due to the different factors may be very destructive and cause harsh effects on the control, rotor position, and performance of ERSRM. Therefore, some methods must be devised to control or compensate the produced forces. In this regard, several studies proposed the search coils which are placed on the stator poles to

produce an additional force on the opposite of radial force direction for compensating it. On the other side, kinds of accelerators are placed on the generator to investigate these forces and their amplitude and then control their values with control unite.

V. CONCLUSION

In this paper, fundamental profiles and the distributions of radial and tangential forces inside the air gap of new external rotor SRM were obtained and analyzed. The results obtained have demonstrated the induced flux to inactive phases in idle mode have very low amplitude, which the produced mutual inductance in the idle phase respect to self-inductance in active phase is 0.7%-4.5% in maximum values. According to the results, it was realized that, the amplitude of radial force was almost zero in low level of forced current. Besides, when the level of forced current was increased from 4 to 5 and 6A, the maximum radial force has 2 and 3 times higher value than 4A current. It can be concluded that the proposed ERSRM is appropriate for various applications in small sizes.

ACKNOWLEDGMENT

This work was supported by a grant (600/1444) from the vice-presidency of research and technology of Shahid Beheshti University.

REFERENCES

[1] H. J. Chen, D. Q. Jiang, and J. Yang et al., "A New Analytical Model for Switched Reluctance Motors," IEEE Transactions on Magnetics, vol. 45, no. 8, pp. 3107-3113, August, 2009.

[2] M. Nguyen, Y. Jung, and H. Yang et al., "Harmonic Intensity Reduction Technique for Single Phase Switched Reluctance Motor Drives Using a New Random PWM Scheme," Journal of Power Electronics, vol. 10, no. 1, pp. 51-57, 2010.

[3] G. J. Li, J. Ojeda, and E. Hoang et al., "Comparative Studies Between Classical and Mutually Coupled Switched Reluctance Motors Using Thermal-Electromagnetic Analysis for Driving Cycles," IEEE Transactions on Magnetics, vol. 47, no. 4, pp. 839 - 847, 2011.

[4] W. Ding, D. Liang, and H. Sui, "Dynamic Modeling and Performance Prediction for Dual-Channel Switched Reluctance Machine Considering Mutual Coupling," IEEE Transactions on Magnetics, vol. 46, no. 9, pp. 3652 – 3663, 2010.

[5] J. Cai, Z. Q. Deng, and R. Y. Qi et al., "A Novel BVC-RBF Neural Network Based System Simulation Model for Switched Reluctance Motor," IEEE Transactions on Magnetics, vol. 47, no. 4, pp. 830 - 838, 2011.

[6] J. Du, D. Liang, and L. Xu et al., "Modeling of a Linear Switched Reluctance Machine and Drive for Wave Energy Conversion Using Matrix and Tensor Approach," IEEE Transactions on Magnetics, vol. 46, no. 6, pp. 1334 - 1337, 2010.

[7] W. Ding and D. Liang, "Modeling of a 6/4 Switched Reluctance Motor Using Adaptive Neural Fuzzy Inference System," IEEE Transactions on Magnetics, vol. 44, no. 7, pp. 1796-1804, 2008.

[8] F. Daldaban and N. Ustkoyuncu, "New Disc Type Switched Reluctance Motor for High Torque Density," Energy Conversion and Management, vol. 48, no. 8, pp. 2424-2431, 2007.

[9] J. H. Park, S. M. Jang, and J. Y. Choi et al., "Dynamic and Experimental Performance of Linear-Switched Reluctance Machine With Inductance Variation According to Airgap Length," IEEE Transactions on Magnetics, vol. 46, no. 6, pp. 2334 – 2337, 2010.

[10] M. D. Hennen and R. W. De Doncker, "Comparison of Outer- and Inner-Rotor Switched Reluctance Machines," in 7th International Conference on Power Electronics and Drive Systems, Thailand, pp. 702-706, 2007.

[11] L. Jiongkang and et al., "Experimental Investigation of In-Wheel Switched Reluctance Motor Driving System for Future Electric Vehicles," in 3rd International Conference on Power Electronics Systems and Applications, PESA, Hong Kong, pp. 1-6, 2009.

[12] D. Wen and L. Deliang, "Modeling of a 6/4 Switched Reluctance Motor Using Adaptive Neural Fuzzy Inference System," IEEE Transactions on Magnetics, vol. 44, no. 7, pp. 1796-1804, 2008.

[13] L. Feng-Chieh and Y. Sheng-Ming, "Instantaneous Shaft Radial Force Control with Sinusoidal Excitations for Switched Reluctance Motors," IEEE Transactions on Energy Conversion, vol. 22, no. 3, pp. 629-636, 2007.

[14] E. Afjei, H. Torkaman, and B. Mazloomnezhad, "A New Double Layer per Phase Configuration for Switched Reluctance Motor," in IEEE International Conference on Power and Energy (PECON), Kuala Lumpur, Malaysia, pp. 222-225, 2010.

[15] E. Afjei and H. Torkaman, "The Novel Two Phase Field-Assisted Hybrid SRG: Magnetio Static Field Analysis, Simulation, and Experimental Confirmation," Progress in Electromagnetics Research B, PIER, vol. 18, pp. 25-42, 2009.

[16] E. Afjei, and H. Torkaman, "Comparison of Two Types of Dual Layer Generator in Field Assisted Mode Utilizing 3D-FEM and Experimental Verification," Progress in Electromagnetics Research B, PIER, vol. 23, pp. 293-309, 2010.

[17] E. Afjei and H. Torkaman, "Finite Element Analysis of SRG under Fault Condition Oriented Towards Diagnosis of Eccentricity Fault," Applied Computational Electromagnetics Society, vol. 26, no. 1, pp. 8-16, 2011.

[18] H. Torkaman, M. S. Toulabi, and E. Afjei, "Electromagnetic Analysis of the Effects of Static Eccentricity Fault on the Radial Force Variations in Switched Reluctance Motors," International Review on Modelling and Simulations, vol. 4, no. 2, pp. 585-590, 2011.

[19] H. Torkaman, E. Afjei, and R. Ravaud et al., "Misalignment Fault Analysis and Diagnosis in Switched Reluctance Motor," International Journal of Applied Electromagnetics and Mechanics, vol. 36, no. 3, pp. 253-265, 2011.

[20] H. Torkaman and E. Afjei, "Magnetostatic Field Analysis and Diagnosis of Mixed Eccentricity Fault in Switched Reluctance Motor," Electromagnetics, Taylor and Francis, vol. 31, no. 5, pp. 368-383, 2011.

[21] H. Torkaman and E. Afjei, "Determining Degrees of Freedom for Eccentricity Fault in SRM Based on Nonlinear Static Torque Function," COMPEL:The International Journal for Computation and Mathematics in Electrical and Electronic Engineering, vol. 30, no. 2, pp. 671-685, 2011.

[22] E. Afjei and H. Torkaman, "Investigation of Electromagnetic Characteristics in External Rotor SRM under Dynamic Eccentricity Fault," International Review of Electrical Engineering, vol. 6, no. 3, pp. 1257-1263, 2011.

[23] H. Torkaman and E. Afjei, "Hybrid Method of Obtaining Degrees of Freedom for Radial Airgap Length in SRM under Normal and Faulty Conditions Based on Magnetiostatic Model," Progress In Electromagnetics Research, PIER, vol. 100, pp. 37-54, 2010.

[24] M. N. Anwar, I. Husain, and A. Radun, "A Comprehensive Design Methodology for Switched Reluctance Machines," IEEE Transactions on Industry Applications, vol. 36, no. 6, pp. 1684-1692, 2001.

[25] Magnet CAD package, "User manual," Infolytica Corporation Ltd., 2007.